Microbubble spectroscopy of ultrasound contrast agents

Sander M. van der Meer and Benjamin Dollet
Physics of Fluids Group, Department of Science and Technology, University of Twente, P.O. Box 217, 7500 AE Enschede, The Netherlands

Marco M. Voormolen, Chien T. Chin,[b] Ayache Bouakaz,[c] and Nico de Jong[d]
Department of Experimental Echocardiography, Erasmus MC, P.O. Box 1738, 3000 DR Rotterdam, The Netherlands

Michel Versluis[a] and Detlef Lohse
Physics of Fluids Group, Department of Science and Technology, University of Twente, P.O. Box 217, 7500 AE Enschede, The Netherlands

(Received 13 July 2006; revised 16 October 2006; accepted 16 October 2006)

A new optical characterization of the behavior of single ultrasound contrast bubbles is presented. The method consists of insonifying individual bubbles several times successively sweeping the applied frequency, and to record movies of the bubble response up to 25 million frames/s with an ultrahigh speed camera operated in a segmented mode. The method, termed microbubble spectroscopy, enables to reconstruct a resonance curve in a single run. The data is analyzed through a linearized model for coated bubbles. The results confirm the significant influence of the shell on the bubble dynamics: shell elasticity increases the resonance frequency by about 50%, and shell viscosity is responsible for about 70% of the total damping. The obtained value for shell elasticity is in quantative agreement with previously reported values. The shell viscosity increases significantly with the radius, revealing a new nonlinear behavior of the phospholipid coating.
 [DOI: 10.1121/1.2390673]

PACS number(s): 43.80.Qf, 43.80.Vj, 43.35.Ei [CCC] Pages: 648–656

I. INTRODUCTION

Medical ultrasound imaging is based on scatter and reflection of sound from inhomogeneities in the tissue.[1] The scatter from blood is much weaker than the scatter from tissue. To increase the scattering properties from the blood pool, an ultrasound contrast agent (UCA) is introduced in the blood. An UCA is a liquid, containing small encapsulated microbubbles, which very efficiently scatter ultrasound.[2–4] In this way, it is possible to visualize and quantify the perfusion of tissue, like for instance the heart muscle, liver, or kidney. Contrast agents are nowadays used in various medical investigations. e.g., in obtaining diagnostic information from the volume and shape of the heart ventricles, or to quantify the perfusion of various organs, like liver or kidney.

The fundamental understanding of the dynamics of contrast bubbles is a field of ongoing research. For example, the quantification of the response of contrast bubbles to ultrasound is an important research aspect. Until now, bubbles are characterized mainly by studying acoustically a representative sample of the UCA, containing many microbubbles.[5–7] From this data the overall resonance behavior of the sample can be deduced. Ideal contrast agents would be monodisperse in size, but in practice they have a size distribution which can be measured with, e.g., a Coulter counter, resulting in a mean size and size range.[8] For SonoVue™ and also for BR-14 (Bracco SA, Geneva), e.g., the mean radius is 1.5 μm, with 95% of the bubbles smaller than 10 μm. The polydispersity of the microbubbles makes it difficult to extract information on the physical properties of single bubbles, since the acoustical response of a bubble strongly depends on its size.[8] Furthermore, the acoustic pressure signal emitted by the bubbles is distorted by frequency dependent scattering and attenuation. On the other hand, measuring the acoustic response of a single individual contrast bubble is a difficult task.[9] First, it is difficult to isolate a single bubble in the focal region of a transducer: this would require at least 1 mm of distance between the bubbles. Second, extracting the absolute pressure emitted by the bubble from the measured response requires an accurate calibration of the transducer transfer function.

To overcome the difficulties associated with acoustical characterization, optical methods have been proposed.[10–14] Such methods are based on the direct measurement of the bubble radius, which, unlike the acoustical response, is not subject to distortion and in principle does not require difficult calibration. Furthermore, the interaction between bubbles (secondary Bjerknes forces) decays as the inverse square of their distance, fast enough to consider different bubbles to oscillate independently as soon as they are separated by a few (roughly ten) bubble radii. Isolating the response of a single bubble optically is thus less constraining than for

[a]Author to whom correspondence should be addressed. Electronic mail: m.versluis@utwente.nl
[b]Present address: Philips Research, Briarcliff Manor, NY.
[c]Present address: Inserm U619, B1A, CHU Bretonneau, 2 bd Tonnell, 37044 Tours Cedex, France.
[d]Also affiliated with: Physics of Fluids Group, Department of Science and Technology, University of Twente, P.O. Box 217, 7500 AE Enschede, The Netherlands.

acoustical measurements. However, optical methods exhibit other drawbacks: very high frame rates are required to resolve microbubble oscillations at several MHz, and the resolution is limited, since the microbubble size is just a little higher than the optical resolution.

Here, we present a new optical method, that we term bubble spectroscopy, to characterize individual contrast bubbles. To resolve the oscillations of such bubbles, we use the ultrahigh speed camera Brandaris,[15] used in a segmented mode described in detail in Sec. II: we scan the insonation frequency to reconstruct a resonance curve, from which we extract the resonance frequency and the total damping coefficient. The experimental methods are detailed in Sec. III. In Sec. IV, we present the main results: we quantify the change of the resonance frequency with the radius, and discuss the influence of shell elasticity. We also quantify damping and show the influence of shell viscosity. We further discuss the accuracy of the proposed method in Sec. V.

II. BUBBLE SPECTROSCOPY

A. The microbubble as a linear oscillator

For small enough acoustic forcing, it is well known[16,17] that a bubble behaves as a linear oscillator; its relative radial excursion x, defined as $R=R_0(1+x)$, obeys the equation

$$\ddot{x} + \omega_0 \delta \dot{x} + \omega_0^2 x = F(t), \tag{1}$$

with $f_0=\omega_0/2\pi$ the eigenfrequency of the system and δ its (linear) dimensionless damping coefficient (equivalently, one can define the quality factor $Q=1/\delta$), and F is the forcing term.

The amplitude of the radial variation of the bubble depends of the driving frequency $f=\omega/2\pi$. Writing $F(t)=F_0 \sin \omega t$ and $x(t)=x_0 \sin(\omega t+\varphi)$, one gets from Eq. (1):

$$x_0(\omega) = \frac{F_0}{\sqrt{(\omega_0^2-\omega^2)^2 + (\delta\omega\omega_0)^2}}. \tag{2}$$

This equation defines the resonance curve, displaying a maximum at the resonance frequency

$$f_{\mathrm{res}} = f_0 \sqrt{1-\frac{\delta^2}{2}}, \tag{3}$$

which is lower than the eigenfrequency in the presence of damping. Strictly speaking, Eq. (3) holds only if the damping coefficient δ is independent of ω. The main objective of our bubble spectroscopy method is to fully characterize the linear response of single bubbles, by constructing its resonance curve and extracting from that the eigenfrequency and the damping coefficient. We show this on a simulation example in the following subsection, and on experiments in Sec. III.

B. Simulation example: Power spectrum and resonance curve

As an example, we derive the resonance frequency and the damping coefficient from a numerical simulation. We compute the time evolution of the radius of a coated bubble subjected to an acoustic pressure, using the following model, adapted from Marmottant *et al.*[18]

$$\rho_\ell \left(R\ddot{R} + \frac{3}{2}\dot{R}^2 \right) = \left[P_0 + \frac{2\sigma_w}{R_0} \right] \left(\frac{R}{R_0} \right)^{-3\gamma} \left(1 - \frac{3\gamma}{c}\dot{R} \right) - P_0 - \frac{2\sigma_w}{R} - 4\chi \left(\frac{1}{R_0} - \frac{1}{R} \right) - \frac{4\mu\dot{R}}{R} - \frac{4\kappa_s \dot{R}}{R^2} - P(t), \tag{4}$$

where R, $\dot{R}$, and $\ddot{R}$ represent the radius, velocity, and acceleration of the bubble wall (R_0 being the equilibrium radius), $\rho_\ell=10^3$ kg/m^3 the volumetric mass of water, $P_0=10^5$ Pa is the ambient pressure and $P(t)$ the driving acoustic pressure, and γ the polytropic exponent; since the oscillations are fast, $\mathrm{Pe}=R_0^2\omega/D_{\mathrm{th}} \gg 1$[18] for bubbles of several microns in size in the MHz regime (here, $D_{\mathrm{th}}=2\times10^{-6}$ m^2/s is the thermal diffusivity of C_4F_{10}), we assume that this exponent equals the ratio of specific heats, $\gamma=1.07$ for C_4F_{10}. Furthermore, $c=1.5\cdot10^3$ m/s is the speed of sound in the fluid, $\sigma_w=0.072$ N/m the surface tension, μ the dynamic viscosity, and $P(t)$ is the acoustic pressure. Equation (4) is based on the Rayleigh-Plesset equation, commonly used to model the behavior of bubbles (see Refs. 19–21 for general reviews on this subject) with two additional parameters to model the shell: an elasticity parameter χ (in N/m), and a shell viscosity κ_s (in kg/s).[27] Various models including the shell properties in the Rayleigh-Plesset equation have already been proposed to model contrast agent bubbles.[13,18,22–26] Most of these models[13,23–25] consider a shell of finite thickness, modeled as a three-dimensional continuous medium, which may not be satisfactory for a monolayer shell. This is why Eq. (4) is inspired from models considering the shell as a two-dimensional viscoelastic medium.[18,26] More precisely, Eq. (4) is closely related to the model of Marmottant *et al.*,[18] who suggested modeling shell elasticity through a radius-dependent surface tension over a certain range of radii (elastic range), below which the bubble buckles and above which the shell breaks. Basically, Eq. (4) would correspond to an infinite elastic range, which is relevant in this study, since we use low enough acoustic pressures to avoid both buckling (associated with nonspherical oscillations) and rupture (which would lead to fast bubble dissolution). Equation (4) is also related to the model of De Jong[22] by a more physical description of radiation and viscous damping. For the sake of simplicity, we account this model for thermal damping as an effective viscosity, taking $\mu=2\times10^{-3}$ Pa s, thus twice that of water.

Linearization of Eq. (4) yields the following eigenfrequency in the elastic regime:

$$f_0 = \frac{1}{2\pi} \sqrt{\frac{1}{\rho R_0^2} \left[3\gamma P_0 + \frac{2(3\gamma-1)\sigma_w}{R_0} + \frac{4\chi}{R_0} \right]}. \tag{5}$$

This eigenfrequency has two contributions: the Minnaert frequency,[28]

$$f_M = \frac{1}{2\pi} \sqrt{\frac{1}{\rho R_0^2} \left[3\gamma P_0 + \frac{2(3\gamma-1)\sigma_w}{R_0} \right]}, \tag{6}$$

i.e., the eigenfrequency of an uncoated bubble, and a shell contribution which increases the eigenfrequency.

The linearization of Eq. (4) also gives the expression of the total damping coefficient: $\delta_{\text{tot}}=\delta_{\text{rad}}+\delta_{\text{vis}}+\delta_{\text{shell}}$, with a contribution coming from the sound reradiated by the bubble, which writes at $\omega=\omega_0$[16]

$$\delta_{\text{rad}}=\frac{\omega_0 R_0}{c}, \tag{7}$$

a viscous contribution

$$\delta_{\text{vis}}=\frac{4\mu}{R_0^2\rho\omega_0}, \tag{8}$$

and a shell viscosity contribution

$$\delta_{\text{shell}}=\frac{4\kappa_s}{R_0^3\rho\omega_0}. \tag{9}$$

To be rigorous, a direct derivation from Eq. (4) gives an expression of δ_{rad} slightly different than the classical expression (7), but the order of magnitude remains the same, and we will see in Sec. IV B that radiation is a secondary contribution to the total damping. We will thus keep the expression (7) for the radiation damping.

We compute Eq. (4) with a bubble of ambient radius $R_0=2.8$ μm. We numerically solve the bubble response $R(t)$ to an ultrasound burst of eight cycles, whose two first and two last cycles are modulated by a Gaussian envelope, as in experiments. The acoustic amplitude is $P_a=1$ kPa to minimize nonlinear effects, and the frequency range was chosen around the estimated resonance frequency, from 1.5 to 2.5 MHz. Next, we apply a fast Fourier transform algorithm on each $R(t)$ curve to compute its Fourier transform, and we take the square of this quantity: we get thus the power spectrum P_R of the radius-time curve. Typical $R(t)$ curves and their corresponding power spectra are shown in Fig. 1. At resonance, more energy goes into the oscillation than off-resonance. We quantify this effect by taking the area in the power spectrum in a band of $\Delta f=175$ kHz around the maximum frequency $f_{\max}$, which we term the response:

$$\text{Re}=\int_{f_{\max}-\frac{1}{2}\Delta f}^{f_{\max}+\frac{1}{2}\Delta f} P_R df.$$

The choice for a value of 175 kHz was found to be a suitable bandwidth for our data analysis. The total area in the power spectrum of the signal is an equivalent measure for the resonance, because nearly all the area in the power spectrum of the signal is located in the fundamental peak. We decided to take the area in a band around the peak, and we checked that the results are indeed in accordance.

We now redetermine the eigenfrequency and the total damping out of the resonance curve, in order to establish and verify the method we want to apply to the experimental data of Sec. III. To do so, we fit the data points to the response of a harmonic oscillator [Eq. (2)], which we rewrite as

$$\text{Re}(f)=\frac{\text{Re}_0}{(1-f^2/f_0^2)^2+(\delta f/f_0)^2}. \tag{10}$$

From the best fit of the data points (shown in Fig. 2 for our simulation example), we extract the eigenfrequency f_0^{fit}

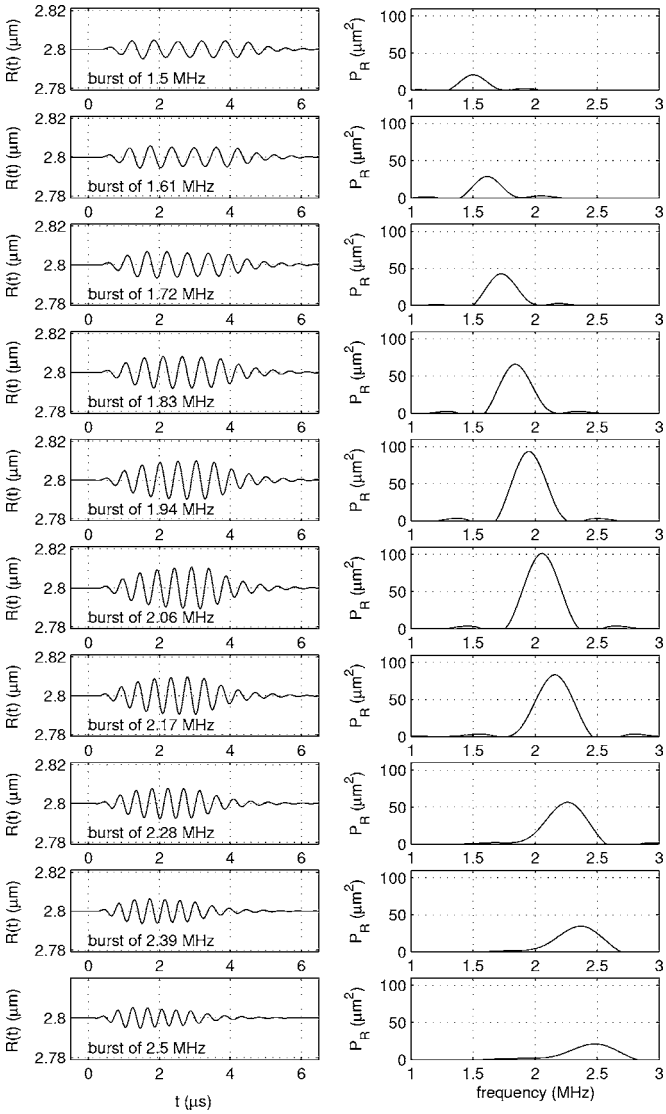

FIG. 1. Simulated response of a bubble of initial radius $R_0=2.8$ μm to an ultrasound wave of 1 kPa of different frequencies. Left: radius-time response; right: power spectrum. The resonance frequency is at 2.07 MHz.

$=2.07$ MHz and the damping coefficient $\delta_{\text{tot}}^{\text{fit}}=0.24$. We will motivate why we analyze the power spectrum, and not directly the radial oscillations, in Sec. III B.

C. Analysis of the resonance curve

From the resonance curve obtained in the simulation example, we can determine the position where the amplitude of the oscillation is maximum, i.e., the resonance frequency: $f_{\text{res}}^{\text{curve}}=2.02$ MHz. The best fit curve to the simulation data displays a resonance frequency compatible within 1% error: $f_{\text{res}}^{\text{fit}}=2.04$ MHz. The resonance frequency is lower than the eigenfrequency $f_0^{\text{fit}}=2.07$ MHz because of damping, but the shift remains very small. The resonance frequencies $f_{\text{res}}^{\text{curve}}$ and $f_{\text{res}}^{\text{fit}}$ fully agree with the theoretical estimate (Table I). Second, the peak width is directly related to the total damping of the system δ_{tot}. A sharp peak indicates low damping, whereas a broad peak indicates high damping. More precisely, the width Δf of the response peak at half the maximum amplitude obeys: $\Delta f/f_0=\delta_{\text{tot}}$. Measuring the width of

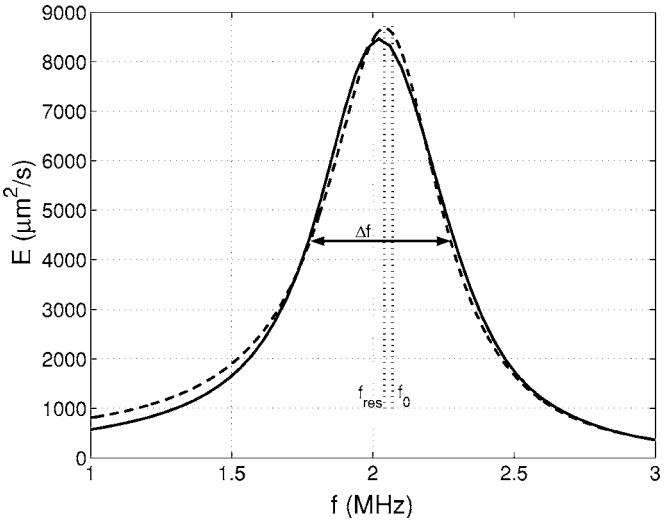

FIG. 2. The simulated response (solid line) of a free 2.8 μm gas bubble on ultrasound bursts of 1 kPa, ranging in frequency from 1 to 3 MHz. The dashed curve is the fit to a harmonic oscillator [Eq. (10)] giving f_0^{fit} =2.07 MHz and $\delta_{\text{tot}}^{\text{fit}}$=0.24.

the peak in Fig. 2 gives the following value for the damping coefficient: $\delta_{\text{tot}}^{\text{curve}}$=0.25, in excellent agreement with the theoretical value: $\delta_{\text{tot}}^{\text{th}}$=0.24 and the value obtained from fit: $\delta_{\text{tot}}^{\text{fit}}$=0.24. This excellent agreement between the theory, the simulation curve, and the fitting curve (Table I) shows that our fitting procedure on the oscillation response is an accurate method to extract both the eigenfrequency and the damping coefficient.

For a linear oscillator, the phase lag φ between the forcing term and the oscillator response is, according to Eq. (1),

$$\tan \varphi = \frac{\delta_{\text{tot}}}{\frac{f_0}{f} - \frac{f}{f_0}}. \tag{11}$$

If the oscillator is driven at frequencies well below resonance, it is in phase with the driving force (φ=0). As the frequency is increased towards resonance, the displacement tends to lag behind the driving, so that at resonance the displacement has a phase shift of $\pi/2$. When the oscillator is driven at frequencies much greater than resonance, the displacement is in antiphase with the driving force ($\varphi=\pi$). In principle, also measuring the phase difference between ultrasound driving and bubble response could be used to determine the resonance frequency of contrast bubbles from experimental data. However, this requires precise timing. Therefore, presently we focus on the oscillation response.

TABLE I. Comparison of the eigenfrequency f_0, the damping coefficient δ_{tot}, and the resonance frequency f_{res} [related through Eq. (3)], from the theory [Eqs. (5)–(9)], the simulation curve, and its fitting curve (Fig. 2).

	f_0 (MHz)	δ_{tot}	f_{res} (MHz)
Theory	2.06	0.24	2.03
Simulation curve	⋯	0.25	2.02
Fitting curve	2.07	0.24	2.04

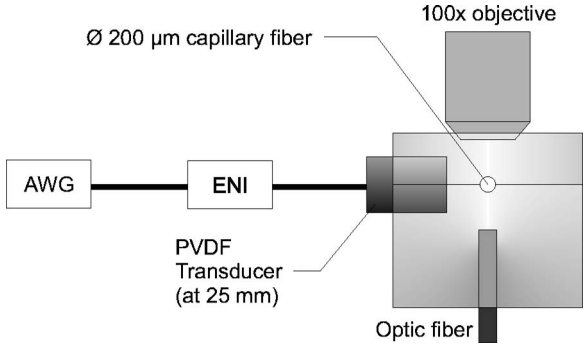

FIG. 3. The experimental setup: an arbitrary waveform generator produces ultrasound signals that are amplified by an amplifier and led to a transducer. Contrast bubbles are injected through a 200 μm capillary fiber perpendicular to the plane of the figure. The contrast bubbles are imaged from the top through a 100× objective and illumination is provided from the bottom.

III. EXPERIMENTS

A. The setup

The experimental setup is schematically drawn in Fig. 3. A dilute solution of individual BR-14 contrast bubbles (Bracco, Geneva) is prepared and injected through a capillary fiber of 200 μm diameter immersed in water. The bubbles are illuminated from below with an optical fiber and an image is produced by an Olympus microscope with a 100× water-immersed objective and a 2× magnifier. We carefully check that only single bubbles are present in the field of view of the microscope. The image is relayed onto a charge coupled device (CCD) camera for orientation and size estimation, and simultaneously onto the Brandaris high-speed camera.[15] The camera can record six movies of 128 frames at up to 25 million frames/s. Furthermore, the camera was designed to operate in a segmented mode, in fact specifically to accommodate microbubble spectroscopy. In practice the conventional single acquisition of 128 frames was replaced by recording two segments of 64 frames each, or four segments of 32 frames each. The camera houses memory space for six conventional acquisitions of 128 frames, before the images are transferred to the PC. Using two segments, this procedure results in the recording of 12 sets of 64 frames. Using four segments has the advantage of an increased frequency resolution (24 instead of 12), but reduces the sampling of the movies from 64 to 32 frames. The camera is operated at a framing rate of 15 million frames/s. The segmented mode allows us to construct a resonance curve of the bubble in a single acquisition, in less than 1 s.

The experiments described here were always done within 6 h after the preparation of the contrast bubbles. The bubbles were introduced through the capillary fiber in the focus of the microscope. Once we identified a single bubble, we estimated its radius from the images of the CCD camera, and estimated its approximate resonance frequency through the Minnaert equation [Eq. (6)], taking into account that the shell elasticity shifts the resonance frequency up. The bubble was then subjected to a scan of 12 (or 24) different frequencies, in a range of roughly 1 MHz below and above the expected resonance frequency. The contrast bubbles were insonified from the side by a broadband single element

transducer (Precision Acoustics, PA081) with a center frequency of 1.7 MHz and a calibrated range of frequencies from 0.7 to 6 MHz. An arbitrary waveform generator (AWG), a Tabor 8026, connected to a PC, was used to produce the required waveforms, which were then amplified by an ENI 350L amplifier. The length of the ultrasound waveforms was eight cycles, of which the first two and the last two were tapered taking a Gaussian envelope. The bubbles were investigated with sequential bursts of the ultrasound waveforms, with an acoustic pressure kept as low as possible to minimize nonlinear responses. In this paper, we present only results at driving pressures lower than 40 kPa. This prevented us from studying bubbles smaller than 1.5 μm in radius, since these bubbles do not oscillate significantly at these small pressures.[40] The pressures generated by the broadband single element transducer were calibrated with a 0.2 mm needle hydrophone (Precision Acoustics, SN1033). To maintain a constant pressure in the focus, we compensated for the frequency-dependent response of the transducer by adjusting the amplitude of the waveforms of different frequencies. The programming of the waveforms was done in MATLAB. The waveforms were transferred to the AWG via a general purpose interface bus (GPIB).

B. Radius-time curves determination

From the images, we extract the radius-time information. The radius-time curves of individual bubbles were measured using a so-called dynamic programming algorithm.[29] The center of the bubble of interest is annotated in the first frame of the recording. This center point was then used to radially resample the bubble and its direct surrounding. The resulting image was used as an input to the algorithm to find the optimal path along the contour of the bubble. After transforming the contour back into the recorded frame the average bubble radius and corresponding center are determined. This center point is then used to repeat the above procedure for the next frame. After running through all frames the radius-time curve of the bubble is obtained. Through a calibration grid the conversion between pixels and micrometers is performed.

To quantify the amplitude of oscillations of a bubble, the simplest method would be to find the maximum and minimum radial excursion during the insonation. However, in experiments, this proved not to be the most accurate measurement for several reasons. First of all, due to the finite sampling frequency of the signal, there is a difference between the recorded extrema and their actual values. Furthermore, the extrema need to be determined from only a few cycles of the bubble oscillation. Second, in experiments an off-resonance oscillating bubble often shows an amplitude overshoot in the first few cycles. Although we tried to minimize this by using a Gaussian envelope, it is somehow arbitrary to choose which of the extrema shows the real amplitude for that particular frequency and pressure. For all these reasons, we rather work on the Fourier transform of the radius-time curve. It also presents a maximum amplitude at resonance, and since it is an integrated quantity over the full $R(t)$ signal, it is much less sensitive to the sampling rate and

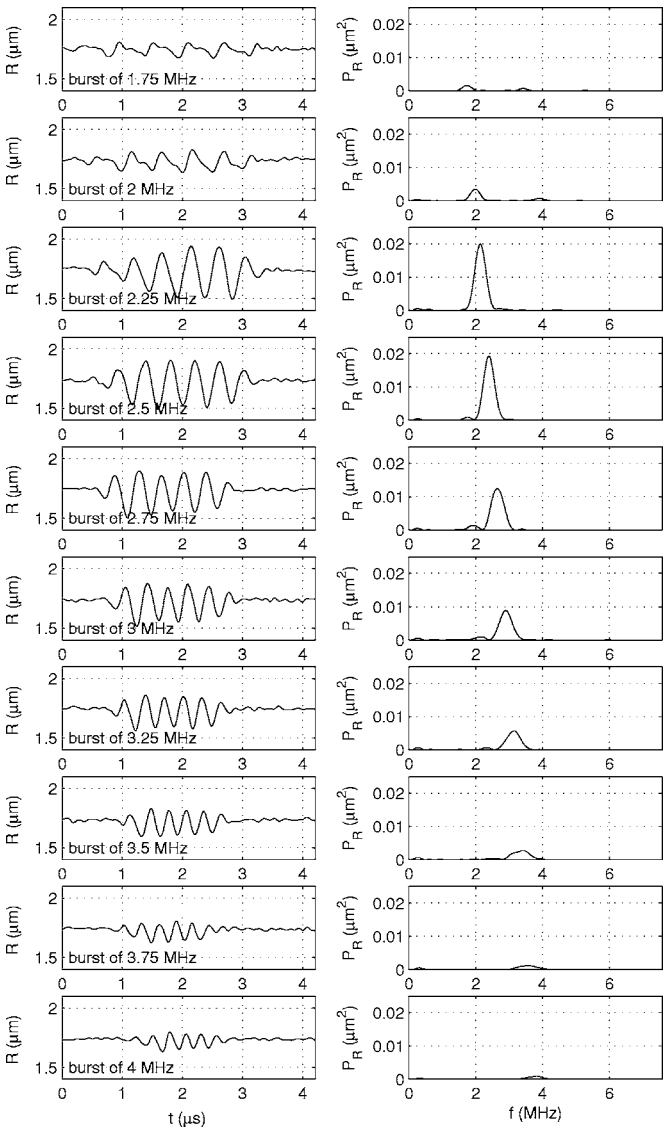

FIG. 4. Experimental radius-time curves (left column), and corresponding power spectra (right column), for a bubble with an ambient radius of 1.7 μm during a scan of insonifying frequencies.

to the short transients and overshoots of the $R(t)$ curve. In the following section we describe the subsequent analysis.

C. Data processing

From the images, the radius-time curves for each individual bubble were measured for each frequency component. An example of such a curve is shown in Fig. 4.

We treat the radius-time curves as in Sec. II B: for each scanned frequency, we calculate the area in the power spectrum in a band around the maximum frequency, as the quantifier of the amplitude of bubble oscillation (Fig. 4). Plotting the results yields an experimental resonance curve which we fit to the linear oscillator expression [Eq. (10)]. Three examples of such resonance curves are displayed in Fig. 5. We then record for each experiment the two following fitting parameters of Eq. (10): the eigenfrequency f_0 and the damping coefficient δ_{tot}. After careful selection (correct pressure, no significant shrinking of the bubble by loss of gas during insonation), we present 22 experimental data points.

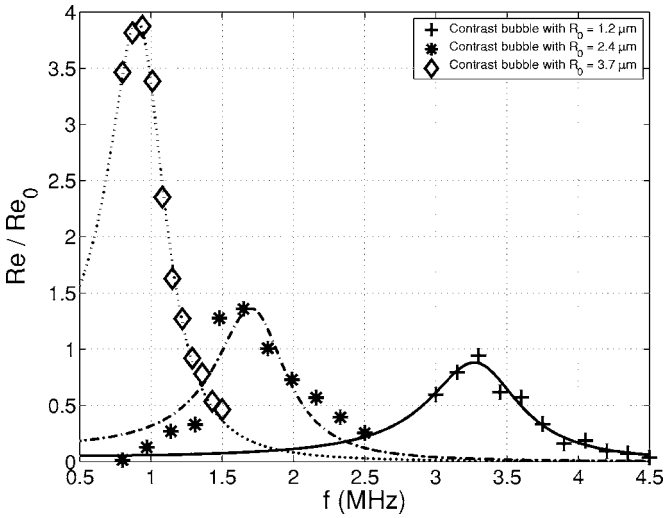

FIG. 5. Experimental resonance curves for three different bubbles, and the corresponding fits by Eq. (10).

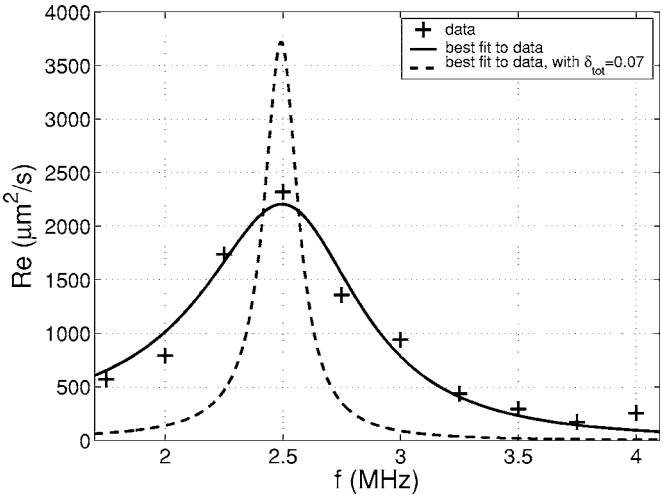

FIG. 7. Example of an experimental resonance curve for a bubble with a resting radius $R_0=1.9$ μm. The solid curve is the fit to Eq. (10), giving $f_0=2.56$ MHz and $\delta_{tot}=0.26$. The dashed line shows the fit to Eq. (10) with an imposed damping coefficient $\delta_{tot}=0.07$ (see text) without shell damping.

IV. RESULTS

A. Eigenfrequency

In Fig. 6, we report the eigenfrequency $f_0=\omega_0/2\pi$, obtained as explained in Sec. III C, for 22 experiments. As expected, the measured eigenfrequencies decrease with the bubble radius. They are also significantly higher than the Minnaert frequency [Eq. (6)], which confirms the influence of the shell. To quantify this influence, we fit the data points to Eq. (5). The best fit yields the following value of the shell elasticity parameter: $\chi=0.54\pm0.10$ N/m, the error bar coming from the dispersion of the experimental data.

The value of χ is fully compatible with the previously reported values for Sonovue™. Using the model of De Jong,[22] which is similar to the model of Marmottant *et al.*[18] used here in the linear regime, Gorce *et al.*[8] gave a value of $\chi=0.55$ N/m based on four analyzed samples. Marmottant *et al.* derived from their model a value of $\chi=1$ N/m on a single example for the shell elasticity.

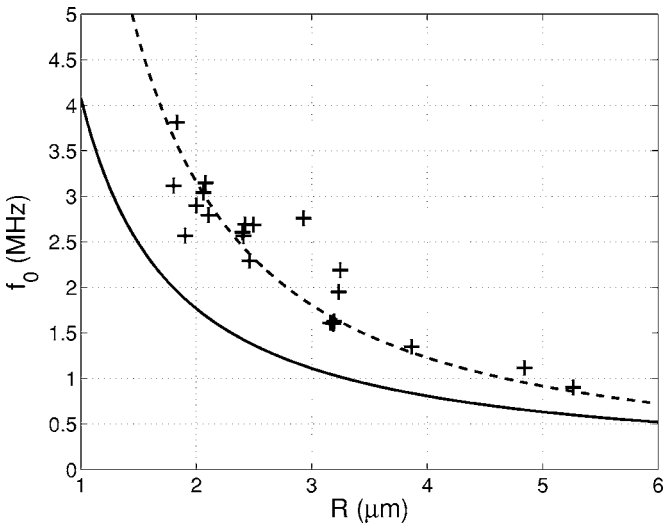

FIG. 6. Experimentally determined eigenfrequency, plotted vs bubble radius. The solid curve shows the Minnaert frequency [Eq. (6)]. The dashed curve shows the resonance frequency including shell elasticity. The best fit with Eq. (5) yields the following value for shell elasticity: $\chi=0.54\pm0.10$ N/m.

B. Damping

We now consider the damping coefficient, which is derived from the experimental data points by fitting to Eq. (10) (see Fig. 5). The damping coefficient is determined as a function of the bubble radius. The variation in the data points is not clearly correlated to the radius, so we rather present a typical example for a bubble of resting radius $R_0=1.9$ μm, see Fig. 7.

Damping arises from various sources: reradiation of sound by the bubbles, thermal diffusion, bulk, and shell viscosity. In the example of Fig. 7, we compute from Eqs. (7) and (8) $\delta_{vis}=0.032$ and $\delta_{rad}=0.022$, given the radius $R_0=1.9$ μm and the eigenfrequency $f_0=2.56$ MHz. Thermal damping is more difficult to express; from Ref. 30 and the value of the thermal diffusivity for C_4F_{10}, we get $\delta_{th}=0.02$. These three sources give a contribution of 0.07 for the damping coefficient. We plot the resonance curve corresponding to this value in Fig. 7: clearly, this curve is too sharp to fit the data correctly, showing the significance of a fourth source of damping, arising from shell viscosity. More precisely, the fit to Eq. (10) with all free parameters gives a significantly higher value of the total damping coefficient, namely $\delta_{tot}=0.26$. This implies a value of $\delta_{shell}=0.19$ for the extra damping through the shell: in this example, shell viscous damping is thus responsible for 73% of the total damping; an average, this proportion is 68%: the shell is therefore the major source of damping. This result confirms existing studies,[31] which showed the significant influence of the shell viscosity on the resonance properties of contrast bubbles. For the total set of 22 data points the value of the shell damping ranged from 0.05 to 0.4. The shell damping shows no clear dependence with the radius, see Fig. 8(A).

From δ_{shell} we can easily calculate the shell viscosity κ_s, see Eq. (9). In the example of Fig. 7, this gives $\kappa_s=2.3\times10^{-8}$ kg/s. Analyzing all data points, we find a significant

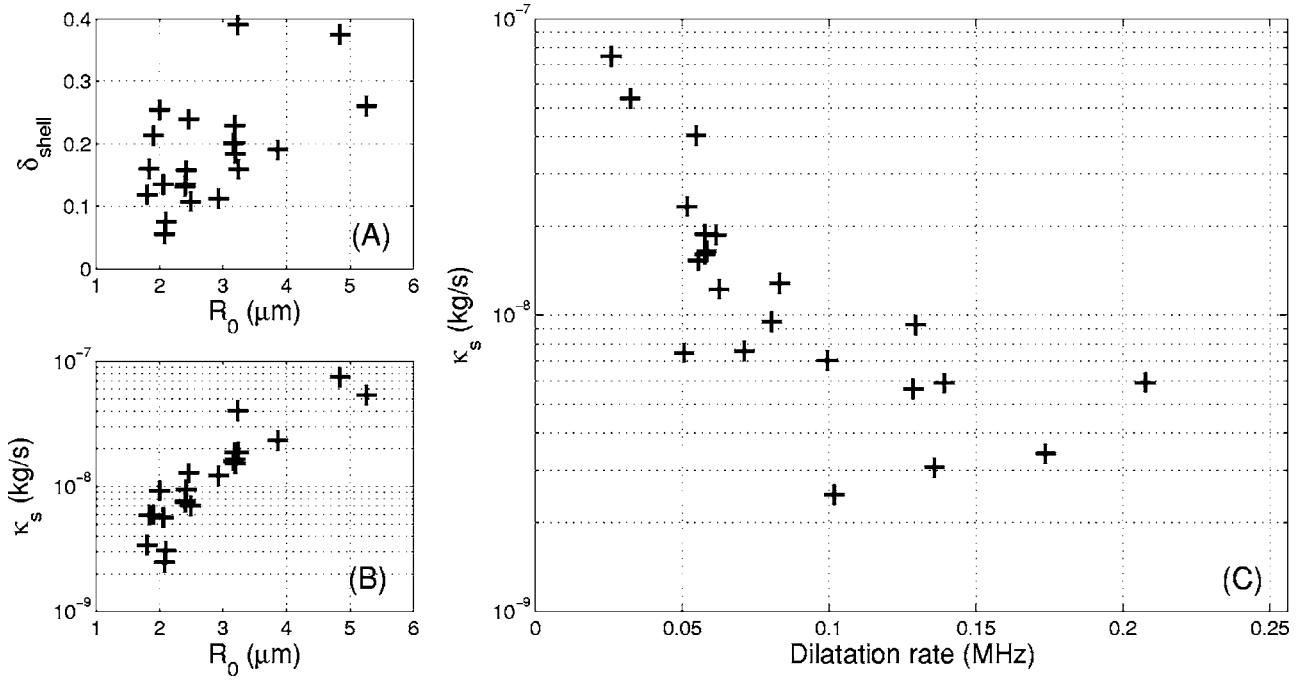

FIG. 8. (A) Experimentally determined shell damping δ_{shell}, plotted vs the ambient bubble radius R_0. (B) Experimentally determined shell viscosity κ_s, plotted vs the ambient bubble radius R_0. (C) Plot of the shell viscosity as a function of the estimate of the dilatation rate $2\pi f_0 \Delta R/R_0$.

increase of the shell viscosity with the radius of the bubble [see Fig. 8(B)], as already reported.[13] However, plotting κ_s as a function of the dilatation rate of the shell offers a more physical picture in terms of surface rheology. We estimate the dilatation rate as: $\dot{R}/R \approx \omega \Delta R/R_0 \approx 2\pi f_0 \Delta R/R_0$, where ΔR is the maximum amplitude of the radial oscillations. We plot κ_s versus the estimated dilatation rate in Fig. 8(C). The plot shows a clear decrease of the shell viscosity with the dilatation rate, which may be the signature of a rheological thinning behavior of the phospholipid monolayer shell. Such a behavior has already been observed for monolayers of myristic acid[32] and of poly(vinylacetate).[33] Furthermore, the order of magnitude of the shell viscosity is 10^{-8} kg/s, which is compatible with previously reported values of $0.72 \cdot 10^{-8}$ kg/s[8]and $1.5 \cdot 10^{-8}$ kg/s.[18]

V. DISCUSSION AND CONCLUSIONS

A. Accuracy of the measurements

We discuss here various sources of bias of the measurements: shrinking of bubbles, compression-only behavior, and uncertainty on the measured radius.

After each burst of ultrasound, some gas may escape from the bubble, reducing the resting radius of the contrast bubble. This unwanted effect is minimized by keeping the ultrasound pressure as low as possible, yet high enough to be able to distinguish the oscillation of the contrast bubble at different frequencies. Great care was taken to verify that the initial resting radius was equal to the final resting radius. In our experiments, we only considered oscillations with a relative decrease in radius less than 10%, hence we assume that the properties of the bubble do not change significantly during the insonation cycle. There is also no difference seen in an ascending or a descending frequency sweep.

Another difficulty is a nonlinear phenomenon referred to as "compression-only" behavior,[34] due to the shell mechanical properties.[18] In the data analysis we included only data for which the ratio between the maximal extension and compression from the equilibrium radius is higher than 0.9: compression only is then negligible.

There is also an uncertainty in the resting radius: since it equals only a few microns, bubbles behave like Mie scatterers[35] hence they create a complicated combination of diffraction and scattering in the focal plane of the camera. This leads to some uncertainty in the image analysis, since the transition in contrast between bubble and background is gradual. The edge detection, described in Sec. III B, at the dark-bright interface at the edge of the bubble will in many cases not give the correct initial bubble radius. Only in the case of in-focus, on-axis, incoherent illumination with a sufficiently high imaging resolution will the lowest cost at the dark-bright interface give the correct bubble radius estimation. In all other cases, the cost needs to be slightly different, depending on the imaging system characteristics like system coherency, objective NA, and abberations (like focus error). In our case we estimate the error we make in the radius estimation at around 10%.

B. Nonlinear pressure and wall effects

The frame rate of 15 million frames/s that was used in the experiment enabled us to resolve the oscillations of the bubbles, to get precise power spectra (Fig. 4), and resonance curves (Fig. 5). We extract a resonance frequency by fitting the observed resonance curves with a linear oscillator response, neglecting the nonlinear influence of the acoustic amplitude, which may be questionable: numerical calculations for uncoated bubbles show that resonance curves be-

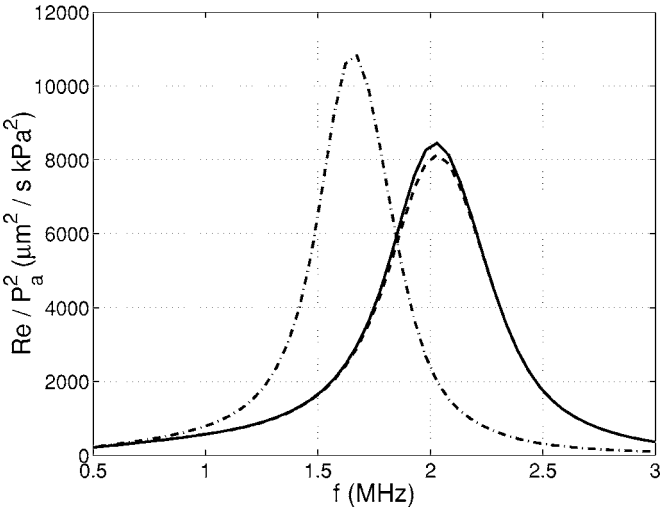

FIG. 9. Resonance curves computed from Eq. (4) for an acoustic amplitude P_a=1 kPa (solid line, same curve as Fig. 2) and 40 kPa (dashed line). Here, the response has been rescaled by P_a^2 to allow for comparison. For P_a =40 kPa we find f_0=2.07 MHz and δ_{tot}=0.24. The third line is a simulation with wall present [dash-dotted line, Eq. (4) computed with an additional term modeling the wall as an image bubble (Ref. 39)]. With wall, we find f_0=1.69 MHz and δ_{tot}=0.21.

come asymmetrical (skewed), and the maximum shifts to a lower frequency. For a driving pressure of 40 kPa the relative decrease of the resonance frequency has been reported to be as large as 10%.[36,37] To address this question for coated bubbles, we perform the same simulation as in Sec. II B with P_a=40 kPa, which is the maximum value used in experiments, and compare the resonance curve with the one of Fig. 2 (see Fig. 9). We find no significant difference, neither in eigenfrequency nor in damping coefficient: the shell elasticity seems to counterbalance the nonlinear effect of pressure.

The presence of the top capillary wall, against which the bubbles rest because of buoyancy, is also expected to affect the resonance frequency.[38,41] As a first approximation, the wall can be modeled as an image bubble, which yields the following prediction of the eigenfrequency of a bubble in contact with a wall: $f_{\text{wall}}=f_0\sqrt{2/3}\simeq 0.82 f_0$.[39] More precisely, we compare the bubble response to an acoustic pressure of amplitude 1 kPa with and without wall in the same figure, Fig. 9. It shows indeed that the eigenfrequency is lowered in the presence of the wall by this factor 0.82. Therefore, the wall tends to lower the resonance frequency; this means that the shell elasticity, 0.54 N/m, that we measured by fitting the experimental data (Fig. 6), is underestimated.

C. Conclusions

We have presented a new, optical method to determine the resonance frequency of individual ultrasound contrast agents bubbles. This method relies on the use of an ultrahigh speed camera, fast enough to resolve bubble oscillations at several Mfps. We operate the camera in a segmented mode, and scan the frequency over the bubble resonance. The bubble response is then recorded at each frequency, and analyzed to construct its resonance curve, from which a resonance frequency as well as a damping coefficient are extracted. The results confirm the influence of the viscoelastic properties of the shell on bubble behavior: The shell elasticity increases the resonance frequency compared to the uncoated bubble case and the shell viscosity proves to be a significant source of damping. Moreover, we showed that the shell viscosity increases with the bubble radius and suggested an explanation in terms of surface rheology.

The measured value of the shell elasticity, 0.54 N/m, and the order of magnitude of the shell viscosity, 10^{-8} kg/s, are in good agreement with previous, independent measurements, giving confidence in this method as an efficient probe of bubble shell properties.

ACKNOWLEDGMENTS

We would like to thank Marlies Overvelde and Jeroen Sijl for fruitful discussions.

This work is part of the research program of the Stichting FOM, which is financially supported by NWO. We acknowledge the Interuniversity Cardiology Institute of the Netherlands (ICIN) and the Senter Novem agency of the Dutch Ministry of Economic Affairs for their financial support. We acknowledge Bracco Research, Geneva, for supplying contrast agents (BR-14 and SonoVue™).

[1] T. Szabo, *Diagnostic Ultrasound Imaging: Inside Out* (Academic, New York, 2004).
[2] N. de Jong, "Acoustic properties of ultrasound contrast agents," Ph.D thesis, Erasmus University Rotterdam (1993).
[3] L. Hoff, *Acoustic Characterization of Contrast Agents for Medical Ultrasound Imaging* (Kluwer, Dordrecht, 2001).
[4] A. L. Klibanov, "Ultrasound contrast agents: Development of the field and current status," Top. Curr. Chem. **222**, 73–106 (2002).
[5] P. J. A. Frinking and N. de Jong, "Acoustic modeling of shell-encapsulated gas bubbles," Ultrasound Med. Biol. **24**(4), 523–533 (1998).
[6] P. J. A. Frinking, N. de Jong, and E. I. Céspedes, "Scattering properties of encapsulated gas bubbles at high ultrasound pressures," J. Acoust. Soc. Am. **105**(3), 1989–1996 (1999).
[7] W. T. Shi and F. Forsberg, "Ultrasonic characterization of the nonlinear properties of contrast microbubbles," Ultrasound Med. Biol. **26**, 93–104 (2000).
[8] J. M. Gorce, M. Arditi, and M. Schneider, "Influence of bubble size distribution on the echogenicity of ultrasound contrast agents. A study of SonoVue™," Invest. Radiol. **35**(11), 661–671 (2000).
[9] S. H. Bloch, R. E. Short, K. W. Ferrara, and E. R. Wisner, "The effect of size on the acoustic response of polymer-shelled contrast agents," Ultrasound Med. Biol. **31**, 439–444 (2005).
[10] J. E. Chomas, P. A. Dayton, D. May, J. Allen, A. L. Klibanov, and K. W. Ferrara, "Optical observation of contrast agent destruction," Appl. Phys. Lett. **77**, 1056–1058 (2000).
[11] N. de Jong, P. J. A. Frinking, A. Bouakaz, M. Goorden, T. Schourmans, J. P. Xu, and F. Mastik, "Optical imaging of contrast agent microbubbles in an ultrasound field with a 100 MHz camera," Ultrasound Med. Biol. **26**, 487–492 (2000).
[12] Y. Sun, D. E. Kruse, P. A. Dayton, and K. W. Ferrara, "High-frequency dynamics of ultrasound contrast agents," IEEE Trans. Ultrason. Ferroelectr. Freq. Control **52**, 1981–1991 (2005).
[13] K. E. Morgan, J. S. Allen, P. A. Dayton, J. E. Chomas, A. L. Klibanov, and K. W. Ferrara, "Experimental and theoretical evaluation of microbubble behavior: Effect of transmitted phase and bubble size," IEEE Trans. Ultrason. Ferroelectr. Freq. Control **47**, 1494–1508 (2000).
[14] P. A. Dayton, J. S. Allen, and K. W. Ferrara, "The magnitude of radiation force on ultrasound contrast agents," J. Acoust. Soc. Am. **112**, 2183–2192 (2002).
[15] C. T. Chin, C. Lancée, J. Borsboom, F. Mastik, M. E. Frijlink, N. de Jong, M. Versluis, and D. Lohse, "Brandaris 128: A digital 25 million frames per second camera with 128 highly sensitive frames," Rev. Sci. Instrum. **74**(12), 5026–5034 (2003).
[16] T. G. Leighton, *The Acoustic Bubble* (Academic, London, 1994).
[17] S. Hilgenfeldt, D. Lohse, and M. Zomack, "Response of bubbles to diag-

nostic ultrasound:A unifying theoretical approach," Eur. Phys. J. B **4**, 247–255 (1998).
[18]P. Marmottant, S. M. van der Meer, M. Emmer, M. Versluis, N. de Jong, S. Hilgenfeldt, and D. Lohse, "A model for large amplitude oscillations of coated bubbles accounting for buckling and rupture," J. Acoust. Soc. Am. **118**(6), 3499–3505 (2005).
[19]M. S. Plesset and A. Prosperetti, "Bubble dynamics and cavitation," Annu. Rev. Fluid Mech. **9**, 145–185 (1977).
[20]C. E. Brennen, *Cavitation and Bubble Dynamics* (Oxford University Press, Oxford, 1995).
[21]M. Brenner, S. Hilgenfeldt, and D. Lohse, "Single bubble sonoluminescence," Rev. Mod. Phys. **74**(2), 425–484 (2002).
[22]N. de Jong, R. Cornet, and C. T. Lancée, "Higher harmonics of vibrating gas-filled microspheres Part one: Simulations," Ultrasonics **32**(6), 447–453 (1994).
[23]C. C. Church, "The effects of an elastic solid surface layer on the radial pulsarions of gas bubble," J. Acoust. Soc. Am. **97**, 1510–1521 (1995).
[24]L. Hoff, P. C. Sontum, and J. M. Havem, "Oscillations of polymeric microbubbles: Effect of the encapsulating shell," J. Acoust. Soc. Am. **107**, 2272–2280 (2000).
[25]D. B. Khismatullin and A. Nadim, "Radial oscillations of encapsulated microbubbles in viscoelastic liquids," Phys. Fluids **14**, 3534 (2002).
[26]K. Sarkar, W. T. Shi, D. Chatterjee, and F. Forsberg, "Characterization of ultrasound contrast microbubbles using in vitro experiments and viscous and viscoelastic interface models for encapsulation," J. Acoust. Soc. Am. **118**(1), 539–550 (2005).
[27]We thank Charles C. Church for pointing out a typo in Ref. 18. The dilatational viscosity κ_s is expressed in units of kg/s.
[28]M. Minnaert, "On musical air-bubbles and the sounds of running water," Philos. Mag. **16**, 235–248 (1933).
[29]M. Sonka, V. Hlavac, and R. Boyle, *Image Processing, Analysis, and Machine Vision*, 2nd ed. (PWS, Pacific Grove, CA, 1999).
[30]A. Prosperetti, "Thermal effects and damping mechanisms in the forced radial oscillations of gas bubbles in liquids," J. Acoust. Soc. Am. **61**, 17–27 (1977).
[31]D. B. Khismatullin, "Resonance frequency of microbubbles: Effect of viscosity," J. Acoust. Soc. Am. **116**, 1463–1473 (2004).
[32]C. Lemaire and D. Langevin, "Longitudinal surface waves at liquid interfaces. Measurement of monolayer viscoelasticity," Colloids Surf. **65**, 101–112 (1992).
[33]F. Monroy, F. Ortega, and R. G. Rubio, "Dilatational rheology of insoluble polymer monolayers: Poly(vinylacetate)," Phys. Rev. E **58**(6), 7629–7641 (1998).
[34]N. de Jong, C. T. Chin, A. Bouakaz, F. Mastik, D. Lohse, and M. Versluis, " 'Compression-only' behavior of phospholipid-coated contrast bubbles," Ultrasound Med. Biol. (in press).
[35]C. F. Bohren and D. R. Huffman, *Absorption and Scattering of Light by Small Particles* (Wiley, New York l983).
[36]W. Lauterborn, "Nonlinear oscillations of gas bubbles," J. Acoust. Soc. Am. **59**(2), 283–293 (1976).
[37]A. Prosperetti, "Bubble phenomena in sound fields: Part two," Ultrasonics **22**, 115–124 (1984).
[38]E. M. B. Payne, S. Illesinghe, A. Ooi, and R. Manasseh, "Symmetric mode resonance of bubbles attached to a rigid boundary," J. Acoust. Soc. Am. **118**, 2841–2849 (2005).
[39]M. Strasberg, "The pulsation frequency of nonspherical gas bubbles in liquids," J. Acoust. Soc. Am. **25**, 536–537 (1953).
[40]J. S. Allen, D. E. Kruse, P. A. Dayton, and K. W. Ferrara, "Effect of coupled oscillations on microbubble behavior," J. Acoust. Soc. Am. **114**(3), 1678–1690 (2003).
[41]M. Emmer, A. van Wamel, D. E. Goertz, and N. de Jong, "The onset of microbubble vibration," Ultrasound Med. Biol. (in press).